AIAA JOURNAL
Vol. 38, No. 9, September 2000

Damping Perturbation Method for Flutter Solution: The *g*-Method

P. C. Chen*
Zona Technology, Inc., Scottsdale, Arizona 85251

By utilizing a damping perturbation method, the present *g*-method includes a first-order damping term in the flutter equation that is rigorously derived from the Laplace-domain aerodynamics. The *g*-method generalizes the K-method and the P–K method for reliable damping prediction. It is valid in the entire reduced frequency domain and up to the first order of damping. The *g*-method utilizes a reduced-frequency sweep technique to search for the roots of the flutter solution and a predictor-corrector scheme to ensure the robustness of the sweep technique. The solution algorithm of the *g*-method is proven to be efficient and robust and can obtain an unlimited number of aerodynamic lag roots, as demonstrated by the results of the selected test cases.

Introduction

SINCE its applicability for flutter analysis was first demonstrated by Irwin and Guyett[1] in 1965, the P–K method has been widely adopted by aeroelasticians as the primary tool for finding flutter solutions. Hassig[2] has given a detailed description of the superiority of the P–K method over the K-method. In Ref. 2, the equation of the P–K method reads

$$\left[(V^2/L^2)\boldsymbol{M}p^2 + \boldsymbol{K} - \tfrac{1}{2}\rho V^2\boldsymbol{Q}(ik)\right]\{\boldsymbol{q}\} = 0 \tag{1}$$

where V is the true speed, L is the reference length, and, usually,

$$L = c/2$$

where c is the reference chord, ρ is the air density, $\boldsymbol{q}$ is the generalized coordinates, and $\boldsymbol{M}$, $\boldsymbol{K}$, and $\boldsymbol{Q}(ik)$ are the generalized mass, stiffness, and aerodynamic forces matrices, respectively.

For simplicity, Eq. (1) excludes the structural modal damping matrix, but it can be easily included. p is the nondimensional Laplace parameter and can be expressed as

$$p = g + ik \tag{2}$$

where k is the reduced frequency,

$$k = \omega L/V$$

ω is the oscillatory frequency, $g = \gamma k$, and γ is the transient decay rate coefficient.

The P–K method is an approximation of the P-method that requires the generalized aerodynamic force computed in the Laplace domain, i.e., $\boldsymbol{Q}(p)$. Because most of the unsteady aerodynamic methods[3–6] used by the aerospace industry are formulated in the frequency domain, i.e., the k-domain, the P–K method can directly adopt $\boldsymbol{Q}(ik)$ from these unsteady aerodynamic methods for flutter calculation.

Rodden[7] modified Hassig's P–K method equation by adding an aerodynamic damping matrix into Eq. (1). The modified P–K method equation reads

$$\left[(V^2/L^2)\boldsymbol{M}p^2 + \boldsymbol{K} - \tfrac{1}{2}\rho V^2(\boldsymbol{Q}^I/k)p - \tfrac{1}{2}\rho V^2\boldsymbol{Q}^R\right]\{\boldsymbol{q}\} = 0 \tag{3}$$

where $\boldsymbol{Q}^R$ and $\boldsymbol{Q}^I$ are the real part and imaginary part of $\boldsymbol{Q}(ik)$, i.e.,

$$\boldsymbol{Q}(ik) = \boldsymbol{Q}^R + i\boldsymbol{Q}^I \tag{4}$$

Received 26 December 1998; presented at the CEAS/AIAA/ICASE/NASA Langley International Forum on Aeroelasticity and Structural Dynamics, Williamsburg, VA, 22–25 June 1999; revision received 1 November 1999; accepted for publication 1 November 1999.

*Vice President, 7430 E. Stetson Drive, Suite 205; pc@zonatech. com.

By substituting $p = g + ik$ into the third term of Eq. (3), this equation can be rewritten as

$$\left[(V^2/L^2)\boldsymbol{M}p^2 + \boldsymbol{K} - \tfrac{1}{2}\rho V^2(\boldsymbol{Q}^I/k)g - \tfrac{1}{2}\rho V^2\boldsymbol{Q}(ik)\right]\{\boldsymbol{q}\} = 0 \tag{5}$$

By comparing Eq. (5) to Eq. (1), it is clearly seen that the extra term

$$-\tfrac{1}{2}\rho V^2(\boldsymbol{Q}^I/k)g$$

is the added aerodynamic damping matrix. Equation (3) is solved at several given values of V and ρ, for complex roots p associated with modes of interest. This is accomplished by an iterative procedure that matches the reduced frequency k to the imaginary part of p for every structural mode. This iterative procedure is called the *reduced frequency "lining-up" process*.[8]

In the following section, we will show that the added aerodynamic damping matrix in Eq. (3) is valid only at small k or for linearly varying $\boldsymbol{Q}(ik)$. The present g-method provides an aerodynamic damping matrix that is valid in the complete k-domain and includes Eq. (3) as a special case.

Formulation of the *g*-Method

The basic premise of the g-method lies in the assumed existence of an analytic function of $\boldsymbol{Q}(p) = \boldsymbol{Q}(g + ik)$ in the domain of $g \geq 0$ and $g < 0$. This premise is based on the fact that the Laplace transform of the time domain unsteady aerodynamics for divergent ($g > 0$) and constant amplitude motions ($g = 0$) is analytic. Because of analytic continuation, $\boldsymbol{Q}(p)$ is also analytic for decay motions ($g < 0$).[9] Thus, $\boldsymbol{Q}(p)$ can be expanded along the imaginary axis, (i.e., $g = 0$), for small g by means of a damping perturbation method:

$$\boldsymbol{Q}(p) \approx \boldsymbol{Q}(ik) + g\left.\frac{\partial\boldsymbol{Q}(p)}{\partial g}\right|_{g=0}, \quad \text{for} \quad g \ll 1 \tag{6}$$

The term

$$\left.\frac{\partial\boldsymbol{Q}(p)}{\partial g}\right|_{g=0}$$

in Eq. (6) is not available from the k-domain unsteady aerodynamic methods. However, if $\boldsymbol{Q}(p)$ is analytic, it must satisfy the Cauchy–Riemann equations such that

$$\frac{\partial[\mathrm{Re}\,\boldsymbol{Q}(p)]}{\partial g} = \frac{\partial[\mathrm{Im}\,\boldsymbol{Q}(p)]}{\partial k} \tag{7}$$

$$\frac{\partial[\mathrm{Im}\,\boldsymbol{Q}(p)]}{\partial g} = -\frac{\partial[\mathrm{Re}\,\boldsymbol{Q}(p)]}{\partial k} \tag{8}$$

Combining Eqs. (7) and (8) yields the following general condition:

$$\frac{\partial\boldsymbol{Q}(p)}{\partial g} = \frac{\partial\boldsymbol{Q}(p)}{\partial(ik)} \tag{9}$$

Equation (9) is valid in the complete p-domain except along the negative real axis where discontinuity due to a branch cut in subsonic flow occurs. Thus, the term

$$\left.\frac{\partial \boldsymbol{Q}(p)}{\partial g}\right|_{g=0}$$

can be replaced by

$$\left.\frac{\partial \boldsymbol{Q}(p)}{\partial g}\right|_{g=0} = \left.\frac{\partial \boldsymbol{Q}(p)}{\partial (ik)}\right|_{g=0} = \left.\frac{\mathrm{d}\boldsymbol{Q}(ik)}{\mathrm{d}(ik)}\right|_{g=0} = \boldsymbol{Q}'(ik) \tag{10}$$

Because $\boldsymbol{Q}(ik)$ can be provided by the k-domain unsteady aerodynamic methods, $\boldsymbol{Q}'(ik)$ can be computed from $\boldsymbol{Q}(ik)$ by a central differencing scheme, except at $k=0$. At $k=0$, a forward differencing scheme is employed to accommodate the discontinuity of $\boldsymbol{Q}(p)$ along the negative real axis. Substituting Eq. (10) into Eq. (6) yields the approximated p-domain solution of $\boldsymbol{Q}(p)$ in terms of k and for small g:

$$\boldsymbol{Q}(p) \approx \boldsymbol{Q}(ik) + g\boldsymbol{Q}'(ik) \tag{11}$$

Replacing $\boldsymbol{Q}(ik)$ in Eq. (1) by $\boldsymbol{Q}(p)$ of Eq. (11) yields the g-method equation:

$$\left[(V^2/L^2)\boldsymbol{M}p^2 + \boldsymbol{K} - \tfrac{1}{2}\rho V^2\boldsymbol{Q}'(ik)g - \tfrac{1}{2}\rho V^2\boldsymbol{Q}(ik)\right]\{\boldsymbol{q}\} = 0 \tag{12}$$

At $g=0$, both the g-method and the P–K method reduce to the same form. This indicates that both methods will provide the same flutter boundary for zero damping. For nonzero g, comparing Eq. (12) to Eq. (5), it can be seen that the difference between the P–K method equation and the g-method equation lies in the terms $\boldsymbol{Q}^I/k$ in Eq. (5) and $\boldsymbol{Q}'(ik)$ in Eq. (12). In fact, $\boldsymbol{Q}^I/k$ is a special case of $\boldsymbol{Q}'(ik)$. This can be shown as follows.

Expanding $\boldsymbol{Q}(ik)$ about $ik=0$ by Taylor's expansion gives

$$\boldsymbol{Q}(ik) = \boldsymbol{Q}(0) + ik\boldsymbol{Q}'(0) + \tfrac{1}{2}(ik)^2\boldsymbol{Q}''(0) + \cdots \tag{13}$$

Because all $\boldsymbol{Q}^n(0)$ are real, $\boldsymbol{Q}(ik)$ can be split into the real and imaginary parts. It reads

$$\boldsymbol{Q}(ik) = \boldsymbol{Q}^R + i\boldsymbol{Q}^I \tag{14}$$

where

$$\boldsymbol{Q}^R = \boldsymbol{Q}(0) - \tfrac{1}{2}k^2\boldsymbol{Q}''(0) + \cdots \tag{15}$$

$$\boldsymbol{Q}^I = k\boldsymbol{Q}'(0) - \tfrac{1}{6}k^3\boldsymbol{Q}'''(0) + \cdots \tag{16}$$

Dividing Eq. (16) by k gives the term $\boldsymbol{Q}^I/k$ in Eq. (5) as

$$\boldsymbol{Q}^I/k = \boldsymbol{Q}'(0) - \tfrac{1}{6}k^2\boldsymbol{Q}'''(0) + \cdots \tag{17}$$

Differentiating Eq. (13) with respect to ik gives the term $\boldsymbol{Q}'(ik)$ in Eq. (12) as

$$\boldsymbol{Q}'(ik) = \boldsymbol{Q}'(0) + ik\boldsymbol{Q}''(0) + \cdots \tag{18}$$

Comparison of Eq. (17) with Eq. (18) shows that the equality of $\boldsymbol{Q}^I/k$ and $\boldsymbol{Q}'(ik)$ exists only if $\boldsymbol{Q}(ik)$ is a linear function of k or at $k=0$. This proves that the added aerodynamic damping matrix in Eq. (5) is valid only if one of these conditions is satisfied. In fact, if $\boldsymbol{Q}(ik)$ is highly nonlinear, the P–K method may produce unrealistic roots because of the error from the differences between Eqs. (17) and (18).

Solution Algorithm of the g-Method

Substituting $p = g + ik$ into Eq. (12) yields a second-order linear system in terms of g:

$$[g^2\boldsymbol{A} + g\boldsymbol{B} + \boldsymbol{C}]\{\boldsymbol{q}\} = 0 \tag{19}$$

where

$$\boldsymbol{A} = (V/L)^2\boldsymbol{M}$$

$$\boldsymbol{B} = 2ik(V/L)^2\boldsymbol{M} - \tfrac{1}{2}\rho V^2\boldsymbol{Q}'(ik) + (V/L)\boldsymbol{Z}$$

$$\boldsymbol{C} = -k^2(V/L)^2\boldsymbol{M} + \boldsymbol{K} - \tfrac{1}{2}\rho V^2\boldsymbol{Q}(ik) + ik(V/L)\boldsymbol{Z}$$

Here, Eq. (19) is formally called the g-method equation. For completeness, in Eq. (19), we have included a modal structural damping matrix $\boldsymbol{Z}$. The solutions of Eq. (19) exist when $\mathrm{Im}(g)=0$. To search for this condition, we first rewrite Eq. (19) in a state-space form:

$$[\boldsymbol{D} - g\boldsymbol{I}]\{\boldsymbol{X}\} = 0 \tag{20}$$

where

$$\boldsymbol{D}\begin{bmatrix} \boldsymbol{0} & \boldsymbol{I} \\ -\boldsymbol{A}^{-1}\boldsymbol{C} & -\boldsymbol{A}^{-1}\boldsymbol{B} \end{bmatrix}$$

and $\{\boldsymbol{X}\}$ is the right eigenvector of the state space equation.

Next, a reduced-frequency-sweep technique is introduced. This technique searches for the condition $\mathrm{Im}(g)=0$ and solves for the eigenvalues of $\boldsymbol{D}$ in term of g; starting from $k=0$, incrementally increasing k by Δk, and ending at $k_{\max}$ ($k_{\max}$ is the highest value in the reduced frequency list of the unsteady aerodynamic computations). The reduced frequency-sweep technique searches for the sign change of the imaginary part of the eigenvalues between k and $|k+\Delta k|$. If this occurs, the condition of $\mathrm{Im}(g)=0$ can be obtained by a linear interpolation in k for the appropriate frequency range. Then the flutter frequency ω_f and damping 2γ are computed by

$$\omega_f = k(V/L) \tag{21}$$

$$2\gamma = 2[\mathrm{Re}(g)/k] \tag{22}$$

For $k=0$, an alternative form of Eq. (22) is used[8]:

$$2\gamma = \frac{\mathrm{Re}(g)(L/V)}{\ell n(2)} \tag{23}$$

One of the issues in performing the reduced frequency-sweep technique is the eigenvalue tracking from k to $|k+\Delta k|$. To monitor the sign change of eigenvalues, it is required that the eigenvalues are lined up at each k and $|k+\Delta k|$. Using the regular sorting scheme by comparing the differences of the eigenvalues at $|k+\Delta k|$ to those at k is certainly not robust and requires small Δk values that may be costly. This eigenvalue tracking issue can be resolved by means of a predictor-corrector scheme.

Predictor-Corrector Scheme for Eigenvalue Tracking

The predictor predicts the eigenvalues at $|k+\Delta k|$ by a linear extrapolation from the eigenvalues and their derivatives at k:

$$g_p(k+\Delta k) = g(k) + \Delta K\frac{\mathrm{d}g}{\mathrm{d}k} \tag{24}$$

where g_p is defined as the predicted eigenvalue. $\mathrm{d}g/\mathrm{d}k$ can be obtained by using the orthogonality property of the left and right eigenvectors of Eq. (20). This leads to

$$\frac{\mathrm{d}g}{\mathrm{d}k} = \left(\boldsymbol{Y}^T\frac{\mathrm{d}\boldsymbol{D}}{\mathrm{d}k}\boldsymbol{X}\right)\Big/\boldsymbol{Y}^T\boldsymbol{X} \tag{25}$$

where $\boldsymbol{Y}$ and $\boldsymbol{X}$ are the left and right eigenvectors of Eq. (20), respectively, and

$$\frac{\mathrm{d}\boldsymbol{D}}{\mathrm{d}k} = \begin{bmatrix} \boldsymbol{0} & \boldsymbol{0} \\ -\boldsymbol{A}^{-1}\dfrac{\mathrm{d}\boldsymbol{C}}{\mathrm{d}k} & -\boldsymbol{A}^{-1}\dfrac{\mathrm{d}\boldsymbol{B}}{\mathrm{d}k} \end{bmatrix} \tag{26}$$

Once g_p is given by the predictor, g_p is used as the baseline eigenvalues for sorting the computed eigenvalues at $|k+\Delta k|$, defined as g_c. The maximum norm of the error between g_p and g_c for all eigenvalues is also computed. If it exceeds a certain level, the

predictor could potentially introduce incorrect eigenvalue tracking results due to rapid changes of the eigenvalues with respect to k in the reduced-frequency-sweep process. In this case, the corrector is activated.

The corrector reduces the size of Δk by a factor, for instance 100, and recomputes g_p and g_c at $(k + \Delta k/100)$ as well as the maximum norm of the error. This process repeats until the maximum norm of the error is below a certain level. However, numerical experience shows that when the corrector is activated, this condition can be satisfied by reducing the size of Δk only once. Therefore, the corrector normally would not increase the computational time significantly. It serves only as a fail-safe scheme.

At $k = k_{\max}$, dg/dk is also used to search for the condition $\mathrm{Im}(g) = 0$ at $k > k_{\max}$ by a linear extrapolation. Thus, the reduced-frequency sweep technique offers a scheme that could find all real roots of Eq. (19) in the complete reduced frequency domain.

At this point, the issue of the number of real roots that could exist in Eq. (19) is discussed. For n structural modes, the P–K method and K-method normally provide only n roots of the flutter equation. However, as indicated by Ref. 10, the number of roots could exceed the number of the structural modes if the aerodynamic lag roots appear. For instance, if the exact Theodorsen function is used, the number of aerodynamic lag roots that would appear is infinite. As one can see, unlike the P–K and K-methods, the reduced-frequency sweep technique employed by the present g-method potentially gives an unlimited number of roots. The inclusion of all activated aerodynamic lag roots could provide important physical insight of the flutter solution

Test Cases and Discussion

The test cases for validating the present g-method are selected from those of the User's Guide of MSC/NASTRAN Aeroelastic Analysis.[11] The generalized aerodynamic forces, mass matrices, and natural frequencies are obtained from MSC/NASTRAN by the Direct Matrix Abstraction Program alter statements. Thus, the difference between the results computed by the P–K method and the g-method is mainly because of the differences in their basic formulation and solution algorithms of these methods.

The 15-Deg Sweptback Wing at $M = 0.45$

This test case is denoted as HA145E in Ref. 11, but with some modifications to produce the P–K method solutions. Four structural modes are used for flutter analysis. The imaginary parts of the 4×4 generalized aerodynamic forces matrix (denoted as $\boldsymbol{Qij}$) vs k are presented in Fig. 1. Because $\mathrm{Im}(\boldsymbol{Qij})$ are all nearly linear, that gives a close equality of Eqs. (17) and (18), the agreement between the damping computed by the P–K method and the g-method is expected. Figure 2 shows the damping vs velocity diagram (v-g diagram) and the flutter frequency vs velocity diagram (v-f diagram) computed by both methods. Good agreement in terms of the overall v-g and v-f comparisons between these methods is obtained, except the g-method predicts one extra aerodynamic lag root (represented by the crosses in Fig. 2). This aerodynamic lag root appears at $V = 595$ ft/s with stable damping but its frequency remains zero. Because the number of roots computed by the P–K method

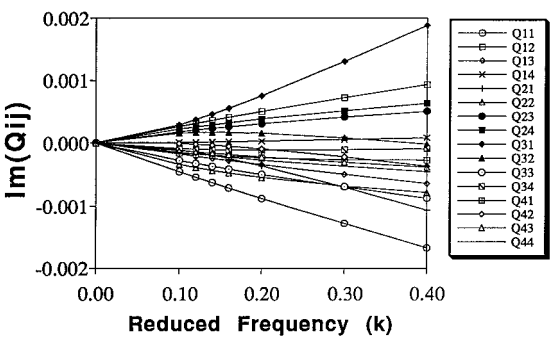

Fig. 1 Generalized aerodynamic forces vs reduced frequency of the 15-deg sweptback wing at $M = 0.45$; four modes.

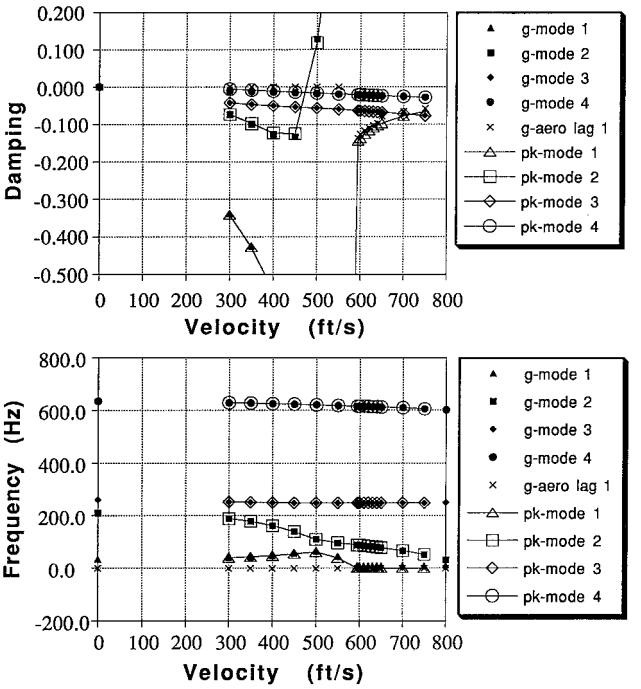

Fig. 2 v-g and v-f diagrams of the 15-deg sweptback wing at $M = 0.45$.

is restricted to be the same as the number of the structural modes, at $V = 595$ ft/s, the P–K method's reduced frequency "lining-up" process skips the bending mode and obtains the aerodynamic lag root. This creates a discontinuity of the damping associated with the bending mode in the v-g diagram (represented by the opened triangles). By contrast, the g-method gives a continuous damping curve of the bending mode (represented by the solid triangles) and a discontinuity in the damping curve of the aerodynamic lag root (the crosses) at $V = 595$ ft/s.

To investigate how the g-method obtains the aerodynamic lag root, the search history in terms of eigenvalues vs k for the reduced frequency-sweep technique is presented in Fig. 3 for $V = 500$ ft/s and Fig. 4 for $V = 650$ ft/s. Because there are four structural modes, the state space form of Eq. (20) provides eight eigenvalues. At $V = 500$ ft/s, the imaginary parts ($\mathrm{Im}(g)$) of these eight eigenvalues provide four zero crossings (marked by the opened circles in Fig. 3a). These four zero crossings represent the four roots of the four structural modes. It is noted that the zero crossing of the first eigenvalue is obtained by extrapolation from the eigenvalue and its derivative at $k = k_{\max}$. At $V = 650$ ft/s $\mathrm{Im}(g)$ of the sixth eigenvalue becomes zero at $k = 0$, which corresponds to the occurrence of the aerodynamic lag root. This can be seen clearly in the expanded view of $\mathrm{Im}(g)$ at small k (at the upper-right-hand corner of Fig. 4a). The real part of this eigenvalue [$\mathrm{Re}(g)$] at $k = 0$ has a negative value (Fig. 4b) that indicates this aerodynamic lag root is stable; however, the expanded view shows a potential coupling between the aerodynamic lag root and the fifth eigenvalue since the zero crossing of the fifth eigenvalue already occurs at small k. This indicates an instability may appear at a higher velocity.

Furthermore, in Figs. 3 and 4, by extrapolating $\mathrm{Im}(g)$ to the negative frequency side, the condition of $\mathrm{Im}(g) = 0$ of other eigenvalues seems to exist. This suggests that at each given velocity, there exist two real roots corresponding to each of the structural mode [(Eq. 19)]. If all these roots were included in the v-g and v-f diagrams (Fig. 2), the aerodynamic lag roots below $V = 595$ ft/s would result in nonzero dampings and associate with negative frequencies. In this case, the corresponding damping curve (g-aero lag 1) in the v-g diagram would be a smooth one. However, its verification is prohibited by the generation of unsteady aerodynamics in the negative frequency domain, a problem that is physically meaningless.

BAH Wing at $M = 0.0$ with 10 Modes

This test case is denoted as HA145b in Ref. 11. Ten structural modes are used for flutter analysis, but only the results of the first

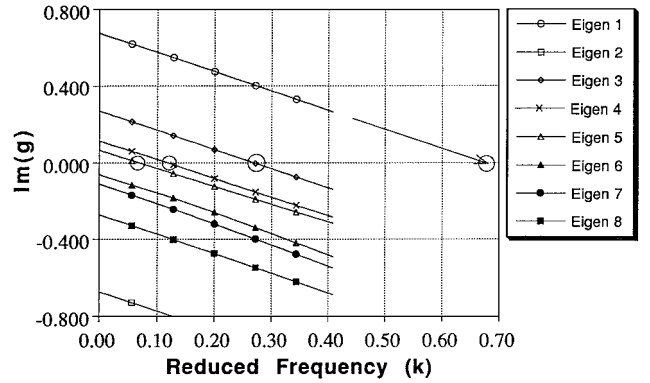

a) Imaginary damping

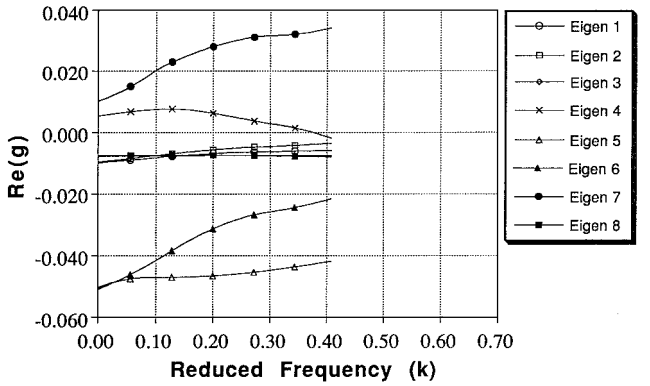

b) Real damping

Fig. 3 Search history of the reduced-frequency-sweep technique at $V = 500$ ft/s.

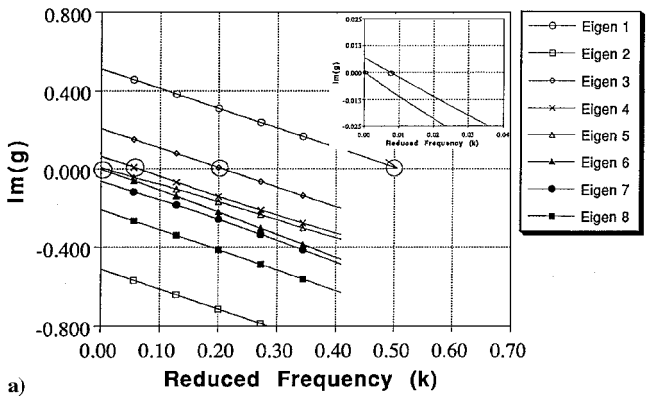

a)

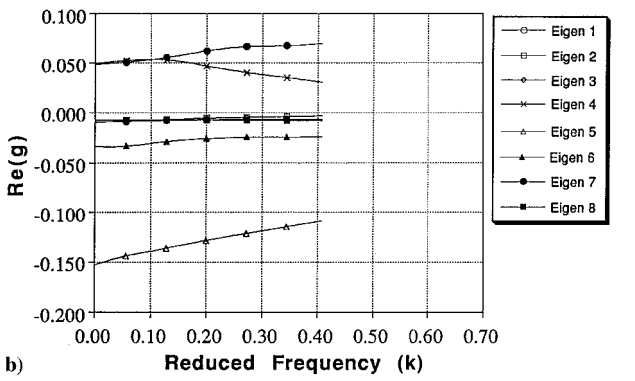

b)

Fig. 4 Search history of the reduced-frequency-sweep technique at $V = 650$ ft/s.

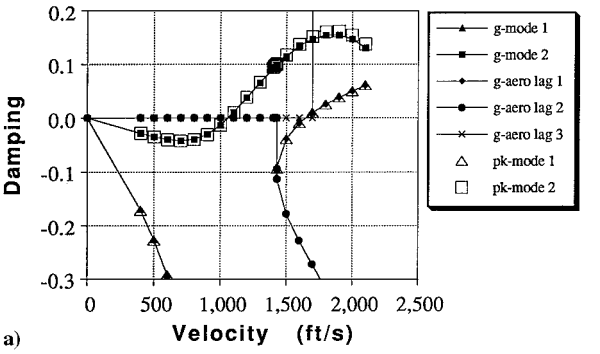

a)

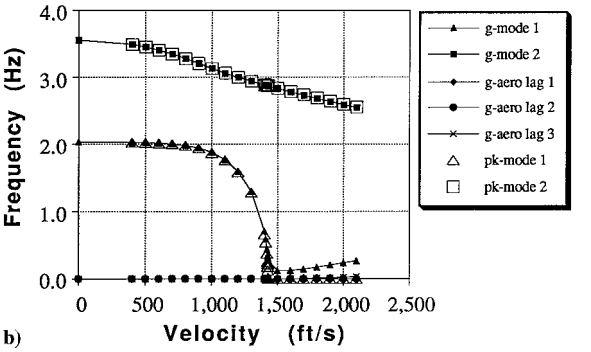

b)

Fig. 5 *v-g* and *v-f* diagrams of the BAH wing: $M = 0.0$, 10 modes.

bending and torsion modes are presented in the *v-g* and *v-f* diagrams shown in Fig. 5. Two types of instability are predicted by both the P–K method and the *g*-method: a flutter speed at $V = 1056$ ft/s and a divergence speed at $V = 1651$ ft/s. This agreement is expected because at $g = 0$ the flutter equation of both methods reduce to the same form. Three aerodynamic lag roots are obtained by the *g*-method and their frequencies are all zero throughout the velocity range of interest. Both of the first and second aerodynamic lag roots appear at the same speed ($V = 1400$ ft/s). Following this speed, the second aerodynamic lag root forms a super-stable mode. At this speed, the damping of the first aerodynamic lag root jumps suddenly from zero to -0.1, then gradually crosses the zero-damping axis, forming a divergence type of instability at $V = 1651$ ft/s. At this divergence speed, the third aerodynamic lag root appears and suddenly jumps to a high value of unstable damping (Fig. 5a). This is an interesting phenomenon because it indicates that this divergence speed could be a bifurcation point. Determining the third aerodynamic lag root is bifurcated from the first aerodynamic lag root or originates on its own needs further investigation.

Similarly to the first test case, the damping curve of the bending mode computed by the P–K method has a discontinuity whereas that of the *g*-method remains a smooth curve. The damping curve of the torsion mode computed by both methods are in excellent agreement. The frequency curves of the two structural modes computed by both methods also in good agreement except for the absence of the three aerodynamic lag roots of the P–K method.

Two-Degree-of-Freedom Airfoil at $M = 0.0$

This test case is adopted from Ref. 10 and is derived from the case denoted as HA145A in Ref. 11, but with the fuselage grid point being constrained. The center of gravity is located at 37% chord. Figure 6 presents the variations of the 2×2 $\boldsymbol{Qij}$ vs k. In this case, Fig. 6 shows that the imaginary parts of $\boldsymbol{Qij}$ is not linear. Therefore, some difference in flutter results between the P–K method and the *g*-method is expected. First, for clarity, the *v-g* diagram computed by the *g*-method alone is presented in Fig. 7. Two aerodynamic lag roots are found. Again, it seems that the second aerodynamic lag root is bifurcated from the first one at $V = 210$ ft/s where a divergence instability occurs. The comparison of the damping and flutter frequencies between the P–K method and the *g*-method is shown in Fig. 8. However, for clarity, the second aerodynamic lag

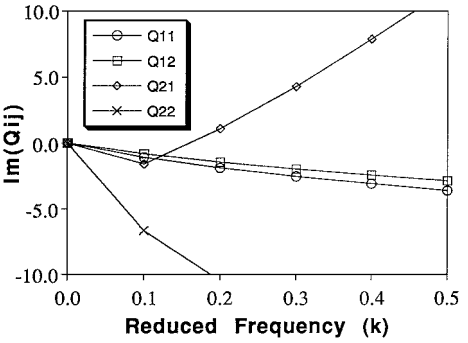

Fig. 6 Generalized forces of two-degree-of-freedom airfoil: c.g. at 37% chord (HA145A1), $M = 0.0$, two modes.

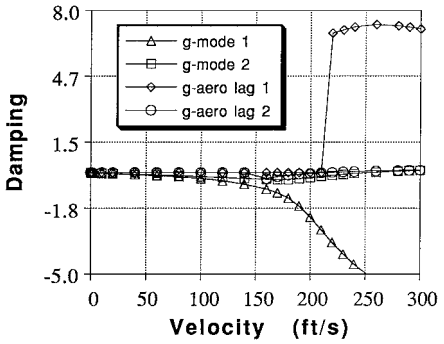

Fig. 7 Two-degree-of-freedom airfoil: c.g. at 37% chord (HA145A1), $M = 0.0$, two modes.

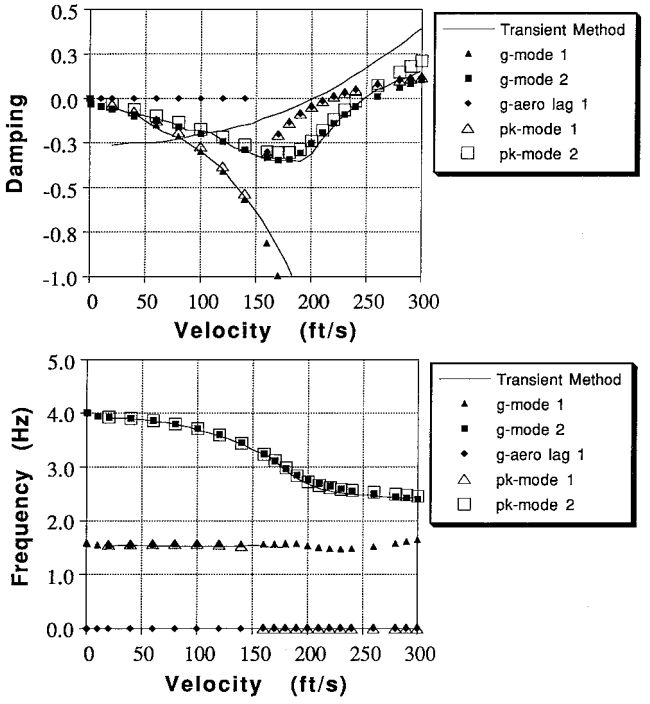

Fig. 8 Damping and frequency vs velocity of two-degree-of-freedom airfoil: c.g. at 37% chord (HA145A1), $M = 0.0$, two modes.

root is not repeatedly shown. In Fig. 8, the results computed by the transient method[12] are also presented. The transient method is based on a time-domain unsteady aerodynamic method; therefore, it can be considered as a p-method. All of the three methods predict the same instabilities: a divergence instability at $V = 210$ ft/s and a flutter instability at $V = 250$ ft/s. The damping curves of the first and second modes computed by the g-method correlate well with those of the transient method. But, again, the P–K method gives a discontinuous damping curve of the first mode.

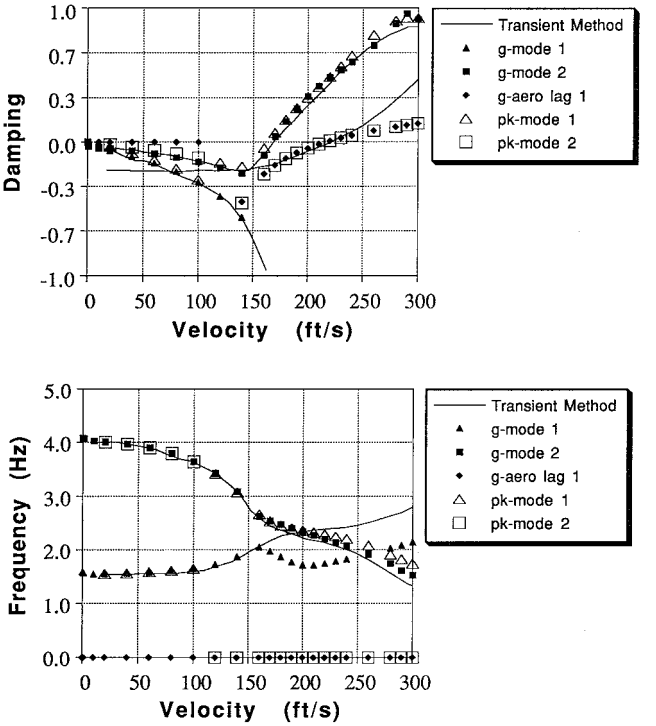

Fig. 9 Damping and frequency vs velocity of two-degree-of-freedom airfoil: c.g. at 45% chord (HA145A2), $M = 0.0$, two modes.

For the case of the center of gravity moved to 45% chord, the v-g diagram shown in Fig. 9 indicates that the flutter instability (at $V = 170$ ft/s) occurs before the divergence instability (at $V = 225$ ft/s). Again, this is well predicted by all three methods. The frequency curves in the v-f diagram computed by the g-method show a similar trend as those of the transient method. But the curves of the P–K method are discontinuous at $V = 100$ ft/s where an aerodynamic lag root appears (not obtained by the transient method but well captured by the g-method). Also, above $V = 100$ ft/s, the P–K method skips the second mode and obtains the aerodynamic lag root. The disappearance of the second mode creates a switch between the first mode and the aerodynamic lag root in the v-f diagram of the P–K method. This results a poor correlation of the v-f curves obtained by the P–K method with the other two methods.

Three-Degree-of-Freedom Airfoil at $M = 0.0$

This test case is denoted as HA145A in Ref. 11. A fuselage free-free plunge mode is added in the two-degree-of-freedom case. The v-g and v-f diagrams for the case of the center of gravity located at 37% chord are shown in Fig. 10 and those for 45% chord are in Fig. 11. For both cases, the so-called "dynamic divergence"[13] occurs and its speeds and frequencies are well predicted by all three methods: the P–K method, the g-method, and the transient method. Both the g-method and the transient method capture one aerodynamic lag root (in the 45% chord case, the g-method obtains two lag roots but one of them appear at the dynamic divergence speed and is not discussed here). Unlike the restrained structures of all previous test cases where the frequency of the lag roots remains zero, the aerodynamic lag root of the present unrestrained structure "takes off" from the zero-frequency axis then couples with the bending mode. This coupling of the lag root and bending mode forms a "dynamic divergence" instability. As indicated by Ref. 13, this dynamic divergence has a nonzero frequency and could be defined as a low-frequency flutter instability. On the other hand, the P–K method generated lag root somehow refuses to "take off" from the zero-frequency axis. This problem of the P–K method is probably due to the fact that because $\boldsymbol{Qij}$ of the present test case is nonlinear, the P–K method is valid only at $k = 0$ for nonzero damping. This $k = 0$ condition restricts the frequency of the lag root from being a nonzero value and results in a poor correlation in the v-f diagram with the other two methods.

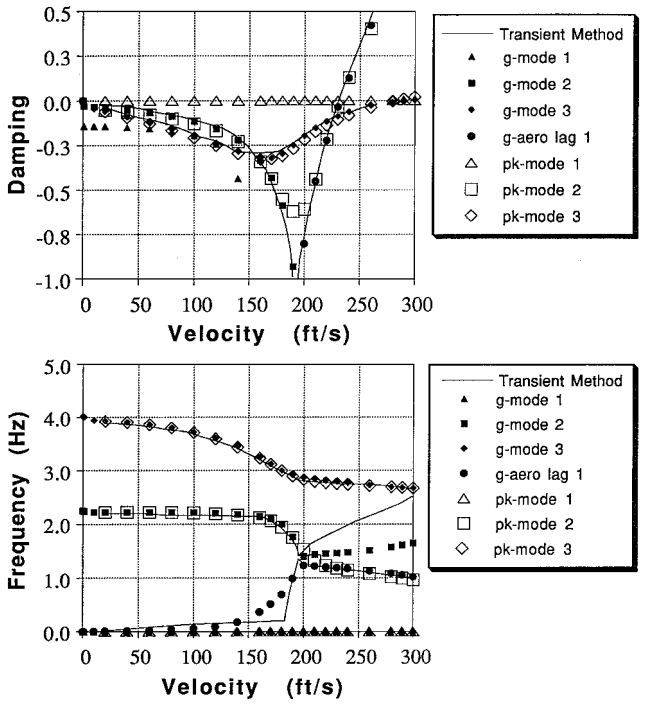

Fig. 10 Damping and frequency vs velocity of three-degree-of-freedom airfoil: c.g. at 37% chord (HA145A2), $M = 0.0$, three modes.

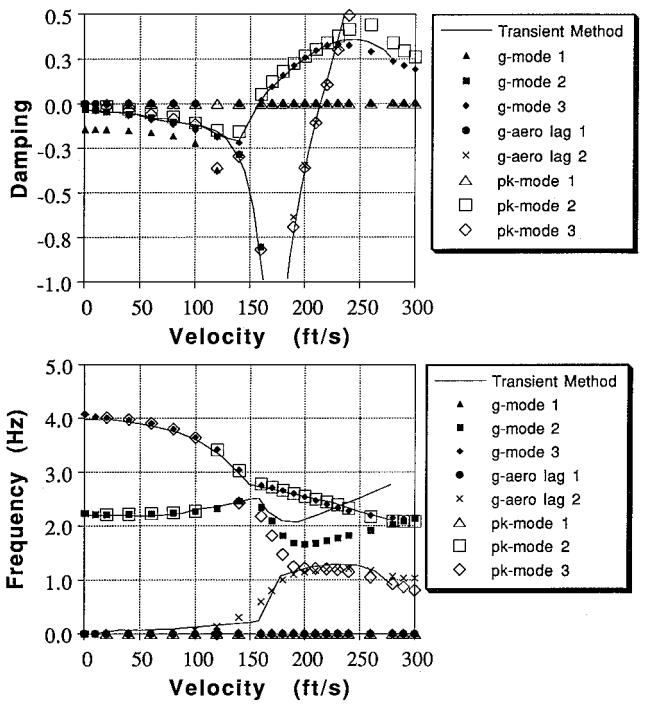

Fig. 11 Damping and frequency vs velocity of three-degree-of-freedom airfoil: c.g. at 45% chord (HA145A2), $M = 0.0$, three modes.

Divergence Speed Due to Lag Root

As mentioned earlier, the inclusion of aerodynamic lag roots could provide important physical insight of the flutter solutions. This can be clearly seen in the BAH wing, two-degree-of-freedom airfoil, and three-degree-of-freedom airfoil cases where both flutter and divergence speed instabilities occur. It is well known that flutter is because of the aeroelastic coupling of structural modes, but the coupling mechanism of the divergence speed instability has not been well understood. The results of these cases computed by the g-method could better clarify this issue.

For the restrained structures such as those in the BAH wing and two-degree-of-freedom airfoil cases, it seems that the divergence speed is a static aeroelastic instability because its associated frequency is zero. However, the results of the g-method suggest that the divergence speed is caused by the coupling of a structural mode and an aerodynamic lag root, and should be considered as a special case of flutter instability. The zero flutter frequency of the divergence speed is caused by the zero-frequency aerodynamic lag root associated with the restrained structure.

For the unrestrained structures like those in the three-degree-of-freedom case, the so-called "dynamic divergence," is again a special case of flutter instability caused by the coupling of the aerodynamic lag root and structural modes but with nonzero frequency. This is supported by the g-method results shown in Figs. 10 and 11, where the frequency coalescence of the bending mode and the aerodynamic lag root is clearly seen. On the other hand, such an interpretation could hardly be supported by the P–K method results because of its incapacity of generating the nonzero-frequency aerodynamic lag root.

Conclusions

It is generally believed that the K-method is valid only at the $g = 0$ condition. The present work also proves that the P–K method is valid when one of the following conditions pertains: (1) $g = 0$, (2) $k = 0$, or (3) $d^n \boldsymbol{Q}/\mathrm{d}k^n = 0$, where $n > 1$. The g-method generalizes the K-method and the P–K method. It is valid for all k and up to the first order of g. This first-order term of g is rigorously derived from $Q(p)$ by a damping perturbation method.

The present work also provides a theoretical foundation for the g-method that can be used to estimate the error of large damping (beyond the first order assumption) because of the truncation of the higher order terms of g. However, based on the formulation of the g-method, adding higher order terms in g seems to be straightforward.

Acknowledgment

The author thanks Professor Gabriel Oyibo for his suggestion in the use of Cauchy–Riemann equations for analytic functions.

References

[1]Irwin, C. A., and Guyett, P. R., "The Subcritical Response and Flutter of a Swept Wing Model," Royal Aircraft Establishment, Rept. 65186, Farnborough, England, U.K., Aug. 1965.

[2]Hassig, H. J., "An Approximate True Damping Solution of the Flutter Equation by Determinant Iteration," *Journal of Aircraft*, Vol. 8, No. 11, 1971, pp. 885–889.

[3]Albano, E., and Rodden, W. P., "A Doublet-Lattice Method for Calculating Lift Distributions on Oscillating Surfaces in Subsonic Flows," *AIAA Journal*, Vol. 7, No. 2, 1969, pp. 279–285.

[4]Chen, P. C., and Liu, D. D., "A Harmonic Gradient Method for Unsteady Supersonic Flow Calculations," *Journal of Aircraft*, Vol. 22, No. 5, 1985, pp. 371–379.

[5]Chen, P. C., and Liu, D. D., "Unsteady Supersonic Computations of Arbitrary Wing-Body Configurations Including External Stores," *Journal of Aircraft*, Vol. 27, No. 2, 1990, pp. 108–116.

[6]Chen, P. C., Lee, H. W., and Liu, D. D., "Unsteady Subsonic Aerodynamics for Bodies and Wings with External Stores Including Wake Effect," *Journal of Aircraft*, Vol. 30, No. 5, 1993, pp. 618–628.

[7]Rodden, W. P., Harder, R. L., and Bellinger, E. D., "Aeroelastic Addition to NASTRAN," NASA CR 3094, 1979.

[8]Rodden, W. P., "Handbook for Aeroelastic Analysis," Vol. 1, MSC/NASTRAN Ver. 65, Nov. 1987.

[9]Stark, V. J., "General Equations of Motion for an Elastic Wing and Method of Solution," *AIAA Journal*, Vol. 22, No. 8, 1984, pp. 1146–1153.

[10]Rodden, W. P., and Bellinger, E. D., "Aerodynamic Lag Functions, Divergence and the British Flutter Method," *Journal of Aircraft*, Vol. 19, No. 7, 1982, pp. 596–598.

[11]Rodden, W. P., and Johnson, E. H., "User's Guide of MSC/NASTRAN Aeroelastic Analysis," MSC/NASTRAN V68, 1994.

[12]Rodden, W. P., and Stahl, B., "A Strip Method for Prediction of Damping in Subsonic Wind Tunnel and Flight Flutter Test," *Journal of Aircraft*, Vol. 6, No. 1, 1969, pp. 9–17.

[13]Rodden, W. P., and Bellinger, E. D., "Unrestrained Aeroelastic Divergence in a Dynamic Stability Analysis," *Journal of Aircraft*, Vol. 19, No. 9, 1982, pp. 796, 797.

A. M. Baz
Associate Editor